MILITARY TECHNICAL COLLEGE
CAIRO - EGYPT

7th INTERNATIONAL CONF. ON
AEROSPACE SCIENCES &
AVIATION TECHNOLOGY

PREDICTION OF RESIDUAL THERMAL STRESSES IN SHORT FIBER - METAL MATRIX COMPOSITES

M. M. MOUSSA* and B. M. RABEEH *

ABSTRACT

Short fiber reinforced metal matrix composites (SFRMMC) were found to be attractive due to the high strength and stiffness, availability and processability at modest cost, machinability and workability, low weight, high temperature serviceability, and microstructure stability . Among the (SFRMMC), the aluminum alloys reinforced with silicon carbide whiskers represent an interesting class. They showed an improvement in strength, stiffness, fatigue and creep of fifty to one hundred percent over unreinforced alloys. A complete understanding of the mechanisms of strengthening and fracture in this class of composites have not yet been established, and a continued detailed studies are required. In the present study the residual thermal stress and strain patterns in the SiC (w) / 6061 Al composites were found to be non-uniform with compressive stresses in the whisker and tensile stresses in the matrix having higher values at the interface and peak values at the whisker end corners, leading to enhanced dislocation generation.

1 . INTRODUCTION AND LITERATURE SURVEY

SFRMMC were found to be attractive due to the high strength and stiffness, availability and processability at modest cost, machinability and workability, low weight, high temperature serviceability, microstructure stability and the documented experimental data on their mechanical properties. Among the (SFRMMC), the aluminum alloys reinforced with silicon carbide whiskers produced from low cost rice hulls represent an interesting class. They showed an improvement in strength, stiffness, fatigue and creep of fifty to one hundred percent over unreinforced alloys [1]. The mechanism of residual thermal stresses is one of the most important mechanisms in strengthening metal matrix composites. The assesment of the development and distribution of the residual thermal stresses and their role in the strengthening of these composites is important. The residual thermal stresses are developed during cooling of the composite from the processing or annealing temperatures due to the large mismatch in the coefficients of thermal expansion between the aluminum matrix and the SiC whiskers. Dislocations punched out from whisker ends during cooling relieve part of the

* Assis. Prof. of Mechanical engg. , Egyptian Armed Forces, Cairo, EGYPT.

residual stresses at the interface. The dislocation punching distance was found to be sufficiently large to cover the majority of the matrix with excess dislocations. The dislocations in the matrix of the composite serve as nucleation sites for strengthening precipitates during the aging of the composite and facilitate the attainment of peak matrix hardness at much shorter times than in the unreinforced matrix alloy. Higher level of dislocations density was observed in the matrix of the composite material than in the unreinforced matrix alloy [2]. Arsenault and Fisher [3] observed a dislocation density of (1-4) x 10^{10} (cm^{-2}) at the interface of both fiber and platelet SiC / 6061 Al composites, and decreases with the distance away from the fibers. Arsenault [4] observed that the level of the strengthening effect of fiber and platelet SiC in aluminum alloy 6061 matrix, was much greater than that predicted by the continuum mechanics theories. Vogelsang et al. [5], using (HVEM), observed a high dislocation density of at least 10^{13} (cm^{-2}), decorated with fine precipitates, in the matrix of annealed whisker and platelet SiC / Al composites at the interface. Control specimens without SiC didn't show dislocations on cooling except at a few large precipitate particles. The quench experiments conducted by Derby and Walker [6] on SiC particulate / Al composites suggest a significant contribution to the strengthening from dislocation generation. As mentioned, the interfacial bond between SiC whiskers and aluminum matrix which contribute to the strength and toughness of the composite is provided by the frictional stresses at the interface which depend on the residual stresses, [7]. Shi et al. [8] indicated that the strengthening of whisker reinforced SiC / Al composite was due mainly to the thermally induced matrix work hardening at the tip of the whisker. Dutta et al. [9] mentioned that for discontinuous SiC whisker reinforced Al - matrix composites, residual stresses were found to significantly affect each of the operative strengthening mechanisms and hence the composite properties. Ho and Saigal [10] found that in casting of SiC /Al particulate-reinforced composites, the matrix undergoes significant plastic deformation during cool down and has higher residual stress distribution as the cooling rate increases. In addition, the presence of thermally induced residual stresses tends to decrease the apparent modulus of elasticity and increase the yield strength of the composites .

2. COMMENTS AND MODEL DESCRIPTION

Several notes concerning the previous models can be drawn :

a - The fiber shape was simplified by a sphere, ellipsoid or an infinitely long cylinder.

b - In most analyses, simple cases of composites were considered and simple models based on Eshelby's equivalent inclusion method were used , considering a single isotropic inclusion embedded in an infinite matrix, thus ignoring the transverse isotropy of the fibers and the interaction between them, and valid only for very small volume fraction of the fibers.

c - Only very few works using three - dimensional thermal stress analysis were performed .

d - One of two hypothetical concepts was usually used in the prediction of the residual stresses The first is the transformation strain applied to the inclusion due to an assumed uniform plastic deformation of the matrix. The second is the Somigliana dislocations at the matrix - fiber interface introduced to accommodate the misfit of thermal expansion coefficients of the matrix and the fiber.

e - Only the stress at a point on the surface of the fiber was predicted and the stress allover the

fiber was assumed to be the same.

f - In most cases , only average stress in the matrix in the region just around the fiber was predicted.

g - The development of residual stresses during cooling was not attempted .

h - No attempt was made to include the heat transfer phase which is very important since it encounter thermal properties like the specific heat and the thermal conductivity of the composite together with the mass density. Instead , a uniform temperature change was assumed.

In the present study the residual thermal stresses developed during cooling from the annealing or processing temperatures for whisker SiC/ 6061 Al alloy composites, for a wide range of whiskers contents and aspect ratios, are predicted. The analysis is performed on continuum mechanics bases, with the aid of a powerful non- linear finite element code [11] , in the meso-scale of a representative unit cell of the composite including one or more inclusions (order of microns). The hexagonal cross-section of the SiC whiskers is simplified by a square cross-section which is more realistic than the circular cross-section used in all the previous studies (Fig. 1, 2). The Structure of the unit cell allows the interaction between whiskers to be accounted for, hence the critical areas of the load transfer and dislocations generation to be mapped. The whiskers are treated as transversely isotropic elastic while the matrix is isotropic elastic - plastic with isotropic hardening behavior. The analysis is three - dimensional and allows the bulk distribution of stresses and strains allover the matrix and the whiskers to be predicted. Transient heat transfer analysis is included in the prediction of the thermal residual stresses, this is important for the accurate prediction of the temperature distribution and history. The average cell dimensions are calculated based on the data given by Arsenault [4] and Nieh [12] for SiC whisker reinforced 6061 Al alloy composites. It was reported that the SiC whiskers derived from the rice hulls are mainly β crystalline structure (cubic) with very small amount of α crystalline structure (hexagonal) present. The whiskers were non - uniformly distributed in the matrix but almost perfectly aligned with their major axes along the extrusion direction. The average cross-section is assumed to be 0.5 x 0.5 (microns), and different whisker lengths 0.9 , 2 , 4 , 6 , 7 (microns) are considered. The whiskers overlap ratio is assumed to be (2/3) and different whiskers weight percents 20 , 25 , 30 , 40 are considered and corresponding volume fractions are calculated. The dimensions of the average cell are calculated for different weight fractions and aspect ratios.

Because of the symmetry in the average cell about the three coordinate planes passing through the origin in the center and about the two diagonal planes , only a representative fraction of the average cell can be used in the analysis (Fig. 3). A mesh used in the finite element analysis is shown in Figure 4 where the most accurate 20 - nodes and 15 - nodes quadratic displacement bricks are used . A central average unit cell , located in the center of the specimen , is considered since the analysis for an arbitrarily located unit cell is rather complicated . A perfect bonding between the matrix and the whisker is assumed based on the results of Flom and Arsenault [13] who reported a value of 1690 (Mpa) for the interfacial bond strength which is 40 times higher than the yield strength of the annealed 6061 Al alloy . The matrix is assumed to be free of voids .

The analysis consists of a transient heat transfer analysis followed by a thermal stress analysis The temperature distribution with time recorded during heat transfer analysis is then used as an input to the thermal stress analysis .

3. TRANSIENT HEAT TRANSFER ANALYSIS

The analysis is based on the energy balance . Equations are derived for the nodal temperature history through the time integration using backward difference algorithm and applying a modified Newton method for the solution of the nonlinear equations . The program uses automatic time stepping to choose the time increment . The temperature history is saved and is used as loading in the thermal stress analysis .

Figure 5 shows the extruded composite specimen as reported by Nieh [12] and Nardone [14]. The mass densities of 6061 Al alloy and SiC whiskers are brought from [15], [16] . The composite density for different SiC weight fractions is calculated . The specific heat and thermal conductivity of both 6061 Al alloy and SiC whiskers [16], [17] are considered . The specific heat and thermal conductivity of the composite are calculated for different SiC weight fractions .

The specimen is initially at a temperature of 450 ° C (.842 ° F) (annealing temperature) . Cooling is assumed to take place by free convection in the air at 21 ° C (70 ° F) (room temperature) . The film coefficients (coefficients of heat transfer from the specimen surfaces) are calculated using the specimen dimensions , the mentioned temperatures and the tables and the procedures outlined by Incropera [18].

Modeling of heat transfer phase is done on the scale of the specimen dimensions to include the heat transfer from the surfaces of the specimen . Hence it is difficult to include the average cell dimensions in this scale to predict the nodal temperature history . A very small element located at the center of the specimen was chosen to simulate the average cell , and is small enough to predict the same temperature at all nodes . The temperatures from the heat transfer analysis are transferred as loading to the corresponding nodes in the thermal stress analysis .

4. THERMAL STRESS ANALYSIS

The transient temperature distribution during heat treatment of materials and the effect of the mismatch in thermal expansion coefficients between the matrix and the whiskers always result in transient stresses large enough to cause plastic flow during the process , thus residual stresses remain after the treatment is completed . The mechanical and thermal properties of the materials are assumed to be temperature dependent ([15], [19] and [20]).

The transversely isotropic elastic behavior of the whiskers can be expressed by the stress - strain - temperature relations in a rate form , assuming the whiskers to be oriented with their axes in the z - direction :

$$\dot{\varepsilon}_{xx} = \frac{\dot{\sigma}_{xx} - \nu\dot{\sigma}_{yy}}{E} - \frac{\nu_{zx}}{E_z}\dot{\sigma}_{zz} + \alpha\dot{T}$$

$$\dot{\varepsilon}_{yy} = \frac{\dot{\sigma}_{yy} - \nu\dot{\sigma}_{xx}}{E} - \frac{\nu_{zy}}{E_z}\dot{\sigma}_{zz} + \alpha\dot{T}$$

$$\dot{\varepsilon}_{zz} = -\frac{\nu_{xz}(\dot{\sigma}_{xx} + \dot{\sigma}_{yy})}{E} + \frac{1}{E_z}\dot{\sigma}_{zz} + \alpha_z\dot{T}$$

$$\dot{\varepsilon}_{xy} = \frac{\dot{\sigma}_{xy}}{2G}; \qquad \dot{\varepsilon}_{yz} = \frac{\dot{\sigma}_{yz}}{2G_z}; \qquad \dot{\varepsilon}_{zx} = \frac{\dot{\sigma}_{zx}}{2G_z} \tag{4.1}$$

where the superposed dot is used for differentiation with respect to time and,

$E = E_x = E_y$, lateral Young's modulus.
E_z , longitudinal Young's modulus.
$\nu = \nu_{xy} = \nu_{yx}$, lateral Poisson's ratio.
$\nu_{zx} = \nu_{zy}$,
$\nu_{xz} = \nu_{yz}$,
$\nu_{zx} / E_z = \nu_{xz} / E$,
$G = G_{xy}$, lateral shear modulus.
$G_z = G_{zy} = G_{zx}$, longitudinal shear modulus.
α , lateral thermal expansion coefficient.
α_z , longitudinal thermal expansion coefficient.

Considering the isotropic behavior of the matrix, it is convenient to decompose the stress and strain tensors, σ_{ij} and ε_{ij}, into their mean parts $(1/3)\sigma_{kk}$ and $(1/3)\varepsilon_{kk}$ and deviatoric parts, s_{ij} and e_{ij}, since the materials are almost perfectly elastic under hydrostatic stress. The mean strain rate is given by:

$$\frac{1}{3}\dot{\varepsilon}_{kk} = \frac{1-2\nu}{3E}\dot{\sigma}_{kk} + \frac{1}{3}\alpha\dot{T} \tag{4.2}$$

where ν is Poisson's ratio, E is Young's modulus, α is the coefficient of linear thermal expansion, and T is temperature.

The deviatoric strain rate can be expressed as the sum of two parts, elastic and plastic :

$$\dot{e}_{ij} = \dot{e}_{ij}^{E} + \dot{e}_{ij}^{P} \tag{4.3}$$

the elastic strain rate is given by:

$$\dot{e}_{ij}^{E} = \frac{\dot{s}_{ij}}{2G} \tag{4.4}$$

where $G = E/2(1+\nu)$, is the elastic shear modulus, and $\dot{s}_{ij}$ is the deviatoric stress rate defined by:

$$\dot{s}_{ij} = \dot{\sigma}_{ij} - \frac{1}{3}\dot{\sigma}_{kk}\delta_{ij} \tag{4.5}$$

The plastic stress-strain relations are given by the temperature dependent von Mises yield condition for hardening solids and the associated flow rules. A detailed discussion of plasticity aspects is given by Prager [21], [22]. The yield condition is in the form :

$$f(s_{ij}, T) = \frac{1}{2}s_{ij}s_{ij} - k^2(T) = J_2 - k^2(T) \tag{4.6}$$

where J_2 is the second invariant of the deviatoric stress tensor and $k(T)$ is the yield stress in simple shear at temperature T. The flow rules associated with this yield condition are :

$$\begin{aligned} &\dot{e}_{ij}^{P} = 0 \quad \text{, if} \quad f < 0 \quad \text{, or if} \quad f = 0, \quad \dot{f} < 0 \\ &\dot{e}_{ij}^{P} = \mu\, s_{ij} \quad \text{, if} \quad f = 0 \quad , \quad \dot{f} \geq 0 \; , \quad \mu = \frac{s_{ij}\dot{e}_{ij}^{P}}{2k^2(T)} \geq 0 \end{aligned} \tag{4.7}$$

where: $\dot{f} = s_{ij}\dot{s}_{ij} - 2k\dot{k}$, $\dot{k} = \frac{dk}{dT}\dot{T}$ (4.8)

Introducing a function $g(x, y, z)$ having a value of zero in the plastic state and a value of one elsewhere; i.e.,

$$\begin{aligned} &g(x,y,z,t) = 1 \text{ , if } \quad f < 0, \text{ or if } \quad f = 0, \quad \dot{f} < 0 \\ &g(x,y,z,t) = 0 \text{ , if } \quad f = 0, \quad \dot{f} \geq 0 \end{aligned} \tag{4.9}$$

Then the stress-strain-temperature relations, equations (4.2 - 4.4 - 4.7 - 4.8) can be combined into the single relation :

$$\dot{\varepsilon}_{ij} = \frac{1+\nu}{E}\dot{\sigma}_{ij} - \delta_{ij}\frac{\nu}{E}\dot{\sigma}_{kk} + \mu\,(1-g)\left(\sigma_{ij} - \delta_{ij}\frac{\sigma_{kk}}{3}\right) + \delta_{ij}\alpha\,\dot{T} \tag{4.10}$$

Equation (4.10) gives for the case of no plastic strain, i.e., $g = 1$:

$$\sigma_{ij} - \frac{\nu}{1+\nu}\delta_{ij}\sigma_{kk} = \frac{E}{1+\nu}\left(\varepsilon_{ij} - \delta_{ij}\,\alpha T\right) \tag{4.11}$$

For the case of plastic strain the yield condition, equation (4.6) gives :

$$\frac{1}{2}\left(\sigma_{ij}-\frac{1}{3}\delta_{ij}\sigma_{kk}\right)\left(\sigma_{ij}-\frac{1}{3}\delta_{ij}\sigma_{kk}\right)=k^2(T)$$

$$\left(\sigma_{ij}-\frac{1}{3}\delta_{ij}\sigma_{kk}\right)\left(\sigma'_{ij}-\frac{1}{3}\delta_{ij}\sigma'_{kk}\right)=kk'(T) \qquad (4.12)$$

so that equations (4.11) and (4.12) can be combined in the following relation :

$$A+B=0 \qquad (4.13)$$

where:

$$A=g\left[\sigma'_{ij}-\frac{\nu}{1+\nu}\delta_{ij}\sigma'_{kk}-\frac{E}{1+\nu}\left(\varepsilon_{ij}-\delta_{ij}\,\alpha\,T\right)\right]$$

$$B=(1-g)\left[\left(\sigma_{ij}-\frac{1}{3}\delta_{ij}\sigma_{kk}\right)\left(\sigma'_{ij}-\frac{1}{3}\delta_{ij}\sigma'_{kk}\right)-kk'\right]$$

The displacement boundary conditions used are that points on a plane of symmetry are restricted from motion in the direction normal to that plane . The tractions on the parallel faces of the cell are assumed to have zero resultant and zero moment . The stress distribution have zero resultant along the coordinate directions . The heated specimen is assumed to be initially stress - free at a temperature of 450° C when cooling begins . Because of the very small size of the average unit cell , all the points will have the same temperature and the temperature will be only a function of time T (t) .

Equations are derived for the time rates of change of the stress components at a time t . These equations express these quantities in terms of the state of stress at time t and the rate of change of the prescribed temperature at that time . The rates of change of the stress components can then be integrated forward to obtain the stress distribution for all times . The above equations together with the boundary , equilibrium and initial conditions and the transient temperature as loading are handled by the ABAQUS program [11] using a step - by - step forward calculation in time to solve for the nodal values of the stresses and strains allover the finite element mesh of the average unit cell .

5. RESULTS AND DISCUSSION

Figures 6 , 7 show the effective residual stresses (compressive) at point C on the whisker surface during cooling for different whiskers weight fractions and aspect ratios . The residual stress at this point decreases with the increase in whiskers weight fraction . This is because the effect of the thermal expansion mismatch should decrease with the decrease in the matrix material which possesses a large coefficient of linear expansion compared to the whisker . With the increase in the whisker aspect ratio , the residual stress was found to increase due to the increase in the shrinkage effect of the whisker which is proportional to its length .

Figure 8 show the residual stresses distribution after cooling along line CL on the whisker surface. The normal stress components in the coordinate directions were found to be compressive allover the whisker except at the whisker end region where some stress components are tensile , specially at point P and its neighborhood . This may be attributed to the effect of the stress concentration at the corners of the whisker ends . The Mises equivalent (effective) stress decreases toward the whisker end due to the whisker shrinkage effects and attains its minimum near the whisker end . The maximum value is attained at the corners of the whisker end (point L) due to the stress concentration at these sharp square corners .

Figures 9 , 10 show the effective residual stresses (tensile) at point L on the matrix surface during cooling for different whiskers weight fractions and aspect ratios . A decrease in the residual stress is observed with the increase in whiskers weight fraction due to the decrease of the effect of thermal expansion mismatch with the decrease of the matrix material . A slight change in the residual stress is observed with the change of the whiskers aspect ratio . The developed residual stresses at this point are shown to exceed the matrix yield strength and yielding of the matrix starts early during cooling (371 - 399 $^{\circ}$ C), leading to dislocations generation .

Figure 11 shows the distribution of residual stresses along line CX in the matrix after cooling . The stress component normal to the interface is compressive while the other two normal components are tensile except at few locations around the whisker end where all the stress components are either tensile or compressive . This fluctuation is due to the stress concentration at the whisker end corners , the mutual interaction between the matrix and whisker and the interaction among whiskers . More details about this fluctuation can be obtained by mesh refinement , although Mises distribution doesn't show any abrupt change . The Mises equivalent (effective) stress exceeds the matrix yield strength (55.2 MPa) allover the interface and in the whisker end region , leading to dislocations generation , and is slightly decreasing in the direction CX with a peak value of (89.7 MPa) at the whisker end , point L , due to the stress concentration there .

Figure 12 shows the residual stresses distribution along line GO after cooling , where the stress in the matrix (line GC) is tensile , while in the whisker (line CO) is compressive . The Mises equivalent (effective) stress in the matrix has a peak value of about (69 MPa) (exceeding the matrix yield strength) at the interface (point C) and decreases away from the whisker . In the whisker , the Mises equivalent (effective) stress has a peak value of about (345 MPa) on the surface (point C) and decreases toward the whisker axis .

Figure 13 shows a schematic of the residual stress distribution in the 6061 Al matrix and the SiC whiskers reported by Arsenault and Taya [23] from the theoretical calculations based on the Eshelby's equivalent inclusion model [24] for ellipsoidal inclusions . The trend of the distribution of the residual stresses agrees with the present predictions .

Figure 14 shows the Mises equivalent residual plastic strain distribution along line CX in the matrix after cooling where a peak , of about 6 % of the matrix strain to failure , is predicted at point L in the whisker end region due to the stress concentration there , giving rise to high dislocation density , and the possibility of interfacial void nucleation and crack initiation .

Figure 15 shows the Mises equivalent residual plastic strain distribution along line GC after cooling where a peak , of about 4 % of the matrix strain to failure , is predicted at point C on the interface and decreases away from it which agrees with the stress distribution and explains the enhanced dislocations density at the interface .

Figures 16 , 17 illustrate the Mises equivalent (effective) residual stress contours in plane GOIQ in the matrix and whisker , respectively , after cooling . In the matrix , high stress is predicted at the interface and decreasing away from it . A peak value for the stress is predicted at the whisker end corner , point L , due to the stress concentration there . In the whisker , high stress is predicted at the whisker surface and decreases toward the whisker axis . Also the stress decreases away from line CO but a peak value is predicted at the corner L due to the stress concentration there , and minimum value is predicted at the region near the whisker end In these figures and the subsequent figures the actual proportions of the matrix and whiskers dimensions are not used , for the sake of viewing more details of the stress and strain patterns

Figures 18 (a ,b) show the Mises equivalent residual plastic strain contours and distribution , respectively , in plane GOIQ in the matrix , after cooling . The whole pattern around a single whisker is shown in Figure 19 . High plastic strain is predicted at the interface and decrease away from it . A peak value , of about 6 % of the matrix strain to failure , is predicted at the corner L due to the stress concentration there . This explains the enhanced dislocations density at the interface and the whisker end , and the crack initiation and void nucleation at the whisker end .

Figure 20 shows the Mises equivalent residual plastic strain contours in plane HOIA in the matrix , after cooling . High plastic strains are predicted at the interfaces and the whiskers corners with a peak value , of about 5 % of the matrix strain to failure , in the area between whiskers . These locations are the expected areas of high dislocations density .

Figure 21 shows the predicted contours of the effective residual stress in the matrix normalized by the room temperature yield strength of 6061 aluminum (283 MPa) , the contours of the effective residual plastic strain in the matrix and contours of the residual axial stress (in MPa) in the SiC whisker , respectively , reported by Povirk et al. [25] . The trend of the distribution of residual stresses and strains in the matrix and the whisker is in agreement with the present prediction .

Figure 22 ([26]) shows a part of the effect of the residual stresses in strengthening the composite , which is the part due to work hardening of the composite by the residual plastic strains . The predicted stress- strain curves for the composite , including residual stresses , are above those for the composite without including residual stresses . For the composite including residual stresses , the compression curve is above the tensile curve due to the tensile residual stresses in the matrix .

Figure 23 ([26]) shows the role of the enhanced dislocations in strengthening the composite . The dislocations in the matrix serve as nucleation sites for strengthening precipitates during

aging of the composite . This strengthening effect can not be predicted by continuum mechanics theories , but it can be observed experimentally as clear from the figure.

The work of Shi et al. [8] is displayed in Figure 24 . The stress-strain curves of a 20 vol. % SiC_w / Al composite with and without thermal history together with that of the annealed 6061 Al are shown. It was found that there is a 50 % increase in the strength of the composite with increasing ΔT .

The work of Dutta et al. [9] is given in Figure 25 . Contours of constant Von-Mises effective stress in 10 vol.% SiC_w / 6061 Al composite due to thermal residual stresses, are shown . A large plastic zone ($\sigma_{eff} \geq 275$ MPa) is observed in the matrix adjacent to the fiber, and some stress concentration evident at the corner of the fiber .

6. CONCLUSIONS

From the present study several important points can be drawn :

1 - The residual stress and strain patterns in the composite are non uniform due to the mutual interaction between the matrix and whiskers , the interaction among the whiskers and the presence of severe stress concentration regions at the whisker corners .

2 - The residual stress in the whisker is compressive with higher values on the surface decreasing toward the whisker axis and toward the whisker ends . The peak value of the effective residual stress is predicted at the corners of the whiskers due to the stress concentration . At the whisker end region , some stress components were found to be tensile due to the severe stress concentration at the corners . The minimum value of the effective stress is predicted at the region near the whisker end .

3 - The residual stresses in the matrix are less affected by the change in the whiskers weight fraction and aspect ratio . High tensile residual stresses in the matrix are predicted at the interface and decrease away from the whisker . These stresses exceed the matrix yield strength so that plastic deformation will take place leading to enhanced dislocations generation . The stress component normal to the interface is compressive while the other two normal components are tensile except at few locations around the whisker end where all the stress components are either tensile or compressive . This is due to the effect of the stress concentration at the sharp square corners of the whisker ends and also due to the mutual interaction between the matrix and whiskers and the interaction among the whiskers . The effective residual stress at the matrix interface is slightly decreasing toward the whisker end with a peak value at the sharp corners at the whisker end due to the stress concentration . High residual stresses were also predicted in the core of the matrix leading to regions of dislocations generation .

5 - The distribution of the Mises equivalent residual plastic strain in the matrix shows higher values at the interface with a peak , of about 6 % of the matrix strain to failure , at the whisker end corners due to the stress concentration there .

6 - High residual plastic strain was predicted in the region between whiskers , giving rise to enhanced dislocations generation which strengthen the matrix at this region , thus become regions of tensile load transfer .

7 - The predicted stress - strain curves for the composite with the residual stresses considered are above those for the composite without considering residual stresses . This strengthening effect is due to the work hardening of the composite by the residual plastic strains . For composites including residual stresses , the compression curve is above the tensile curve due to the tensile residual stresses in the matrix . A significant strengthening of the composite is caused by the enhanced dislocations in the matrix serving as nucleation sites for strengthening precipitates during aging . This strengthening is observed experimentally and not by predictions based on continuum mechanics theories .

REFERENCES

[1] Rack , H . J ., Baruch , T . R . and Cook , J . L . (1982) , " Mechanical Behavior of Silicon Carbide Whisker Reinforced Aluminum Alloys ,'' *Progress in Science and Engineering of Composites* , T . Hayashi, K . Kawatawa and S . Umekawa Ed ., ICCM - IV , Tokyo , pp. 1465 - 1472 .

[2] Christman, T. and Suresh, S. (1988), " Microstructural Development in an Aluminum Alloy - SiC Whisker Composite,'' *Acta Metall.*, Vol. 36, No. 7, pp. 1691-1704.

[3] Arsenault , R. J. and Fisher, R. M. (1983), " Microstructure of Fiber and Particulate SiC in 6061 Al Composites, ''*Scripta Metallurgica*, Vol. 17 , pp. 67-71 .

[4] Arsenault , R. J. (1984), " The Strengthening of Aluminum Alloy 6061 by Fiber and Platelet Silicon Carbide, '' *Materials Science and Engineering* , Vol. 64, pp. 171-181.

[5] Vogelsang, M., Arsenault, R. J. and Fisher, R. M. (1986), " An In Situ HVEM Study of Dislocation Generation at Al / SiC Interfaces in Metal Matrix Composites, '' *Metall. Trans.*, Vol. 17A, March 1986, pp. 379-388.

[6] Derby, B. and Walker, J. R. (1988), " The Role of Enhanced Matrix Dislocation Density In Strengthening Metal Matrix Composites,'' *Scripta Metallurgica*, Vol. 22, pp. 529-532.

[7] Majumdar, S., Kupperman, D. and Singh, J. (1988), " Determination of Residual Thermal Stresses in a SiC-Al_2O_3 Composite Using Neutron Diffraction, '' *J. Am. Ceram. Soc.*, Vol 71, No. 10, pp. 858-863.

[8] - Shi, N., Wilner, B. and Arsenault, R. J. (1992), " An FEM Study Of The Plastic Deformation Process Of Whisker Reinforced SiC / Al Composites'' *Acta Metall. Mater.* Vol. 40, No. 11, pp. 2841-2854.

[9] - Dutta, I., Sims, J. D. and Seigenthaler, D. M. (1993), "An Analytical Study Of Residual Stress Effects On Uniaxial Deformation Of Whisker Reinforced Metal-Matrix Composites '' , *Acta Metall. Mater.* Vol. 41, No. 3, pp. 885-908.

[10] - Ho, S. and Saigal, A. (1994), " Three-Dimensional Modeling Of Thermal Residual Stresses And Mechanical Behavior Of Cast SiC Al Particulate Composites'', *Acta Metall. Mater.* Vol. 42, No. 10, pp. 3253-3262.

[11] *ABAQUS Theory Manual* , Hibbit , Karlson and Sorensen , Inc ., October 1983 .

[12] Nieh, T. G. (1984), " Creep Rupture of a Silicon Carbide Reinforced Aluminum Composite ,''*Metall. Trans.*, Vol. 15A, pp. 139-145.

[13] Flom, Y. and Arsenault, R. J. (1986), " Interfacial Bond Strength in an Aluminum alloy 6061-SiC composite, '' *Materials Science and Engineering*, Vol. 77, pp. 191-197.

[14] Nardone, V. C. and Strife, J. R. (1987), " Analysis of the Creep Behavior of Silicon Carbide Whisker Reinforced 2124 Al (T 4), '' *Metall. Trans.*, Vol. 18A, pp. 109-114.
[15] *Metals Handbook, Ninth Edition*, Vol. 2, 1979.
[16] *Handbook of Chemistry and Physics*, 1984-1985.
[17] *JANAF Thermochemical Tables, Third Edition, Part I, II, J. Physical and Chemical Reference Data.*
[18] Incropera, F. P. and De Witt, D. P. (1981), Fundamentals of Heat Transfer , Ed. J. Wiley and Sons Inc.
[19] *Aerospace Structural Metals Handbook* , 1989 .
[20] *Handbook of Structural Alloys*, 1990.
[21] Prager , W . (1957), " An Introduction to the concepts and principles of Plasticity,'' special lectures delivered at the seminar in Applied Mathematics, Boulder, Colo., July 1957.
[22] Prager , W . (1957), " Non - Isothermal Plastic Deformation, '' Brown University, Technical Report No. 526 (02) / 4, November , 1957 .
[23] Arsenault, R. J. and Taya, M. (1987), " Thermal Residual Stress In Metal Matrix Composite,'' *Acta Metall.*, Vol. 35, No. 3, pp. 651-659.
[24] Eshelby, J. D. (1957), " The Determination of The Elastic Field of an Ellipsoidal Inclusion, and Related Problems,'' *Proc. Roy. Soc. London*, Vol. 241A, pp. 376-396.
[25] Povirk , G. L. , Needleman , A. and Nutt , S. R. (1990) , "An Analysis of Residual Stress Formation in Whisker - reinforced Al - SiC composites , '' *Materials Science and Engineering*, Vol. 125A, pp. 129 -140.
[26] Moussa, M. M. (1990) , " Prediction of The Behavior of Short - Fiber Metal Matrix Composites Using 3-D Nonlinear Finite Element Analysis '' Ph.D Thesis , Illinois Institute of Technology , Chicago .

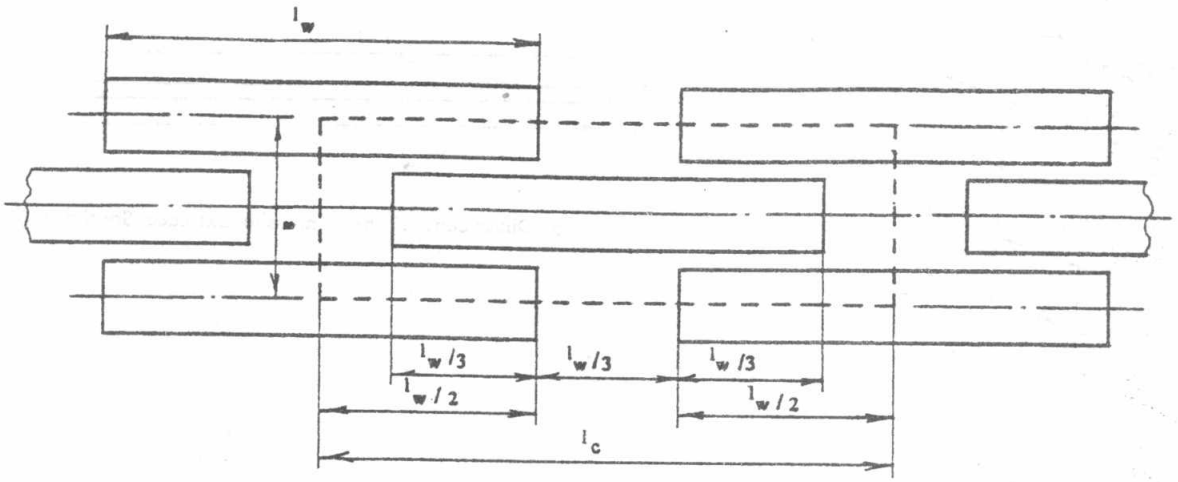

Figure 1. Whiskers Arrangement and Average Cell Borders (aspect ratio=6, SiC wt.%=20).

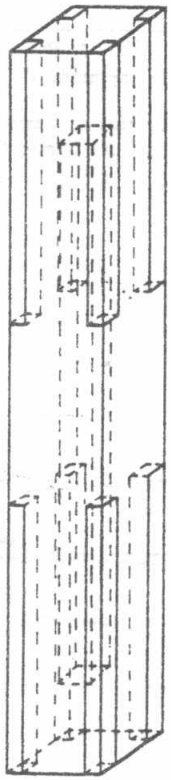

Figure 2. Average Cell Structure (aspect ratio=17, SiC wt.%=20).

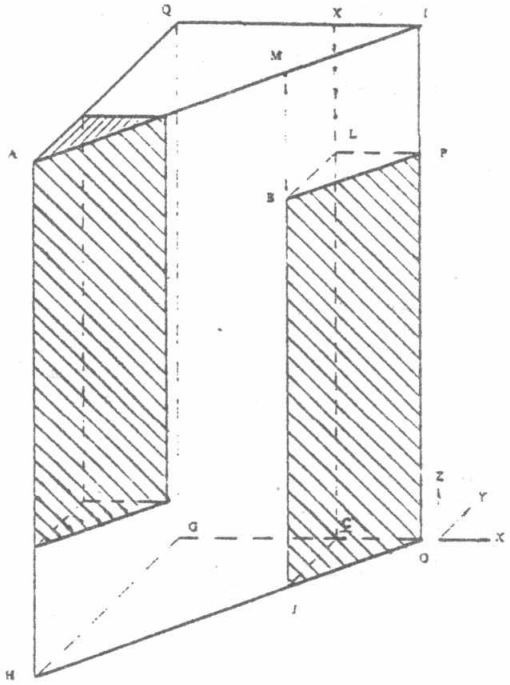

Figure 3. A Representative Fraction of the Average Cell (aspect ratio=4, SiC wt.%=20)

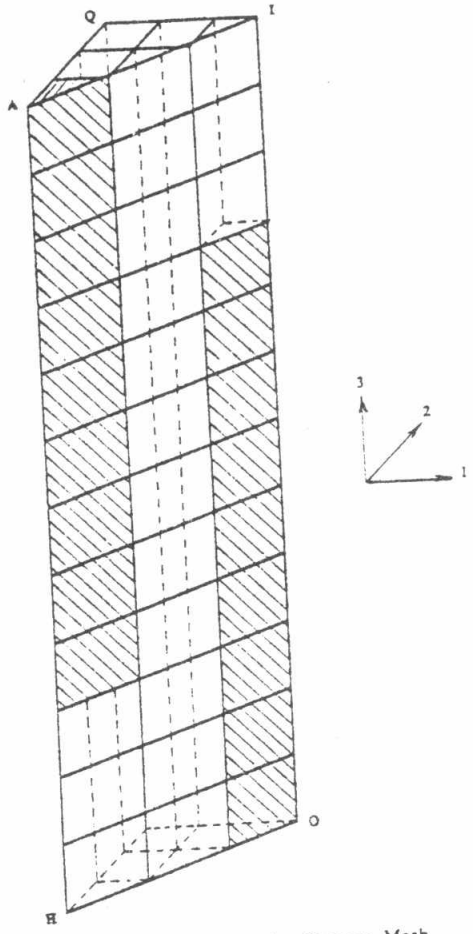

Figure 4 Meso-scale Finite Element Mesh (aspect ratio=12, SiC wt.%=20).

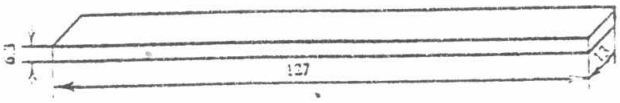

Figure 5. Dimensions of the Composite Extruded Specimen (mm)

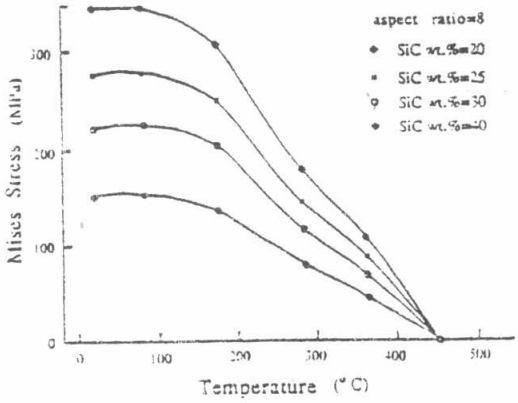

Figure 6 Development of Residual Stress at Point C (on the Whisker Surface) During Cooling.

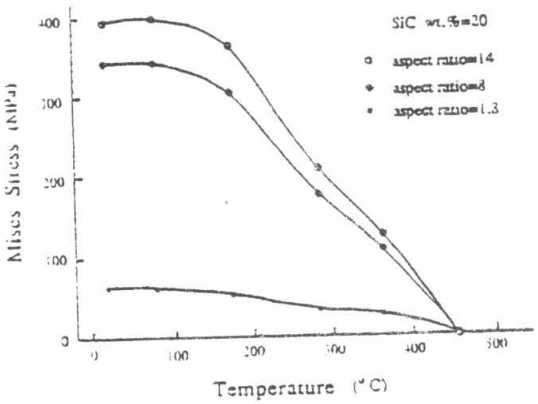

Figure 7 Development of Residual Stress at Point C (on the Whisker Surface) During Cooling.

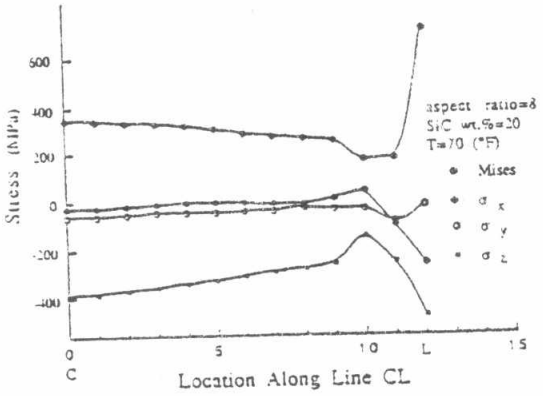

Figure 8. Residual Stresses Distribution Along Line CL (on the Whisker Surface) After Cooling.

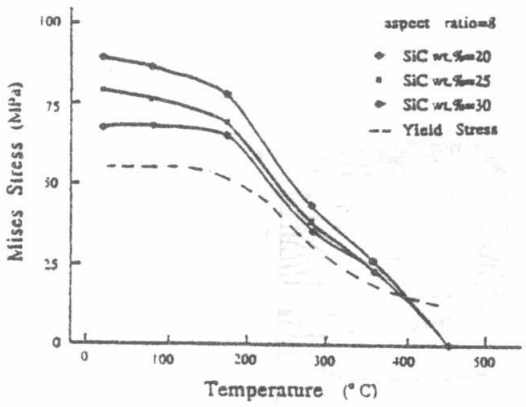

Figure 9 . Development of Residual Stress at Point L (on the Matrix Surface) During Cooling.

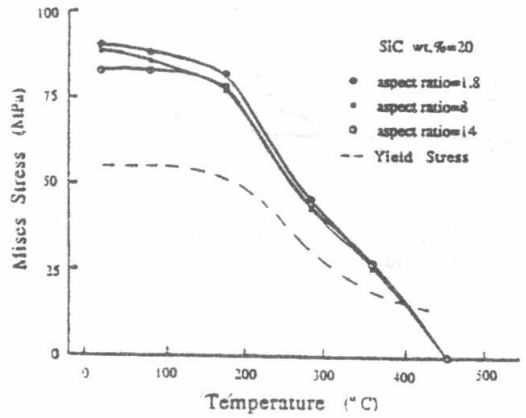

Figure 10 Development of Residual Stress at Point L (on the Matrix Surface) During Cooling.

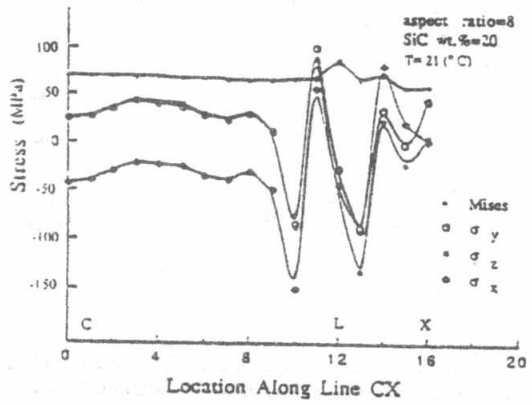

Figure 11 . Residual Stresses Distribution Along Line CX (in the Matrix) After Cooling.

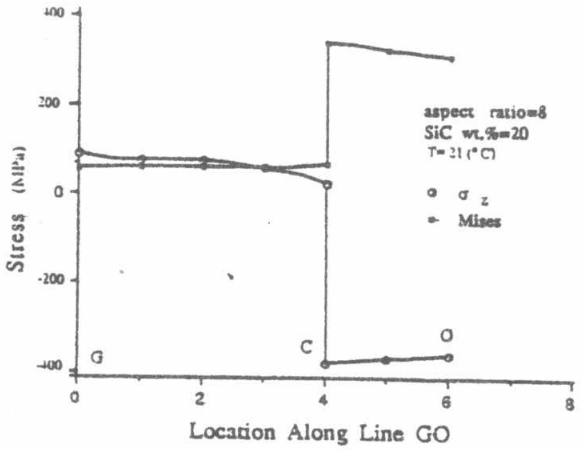

Figure 12 Residual Stresses Distribution Along Line GO After Cooling.

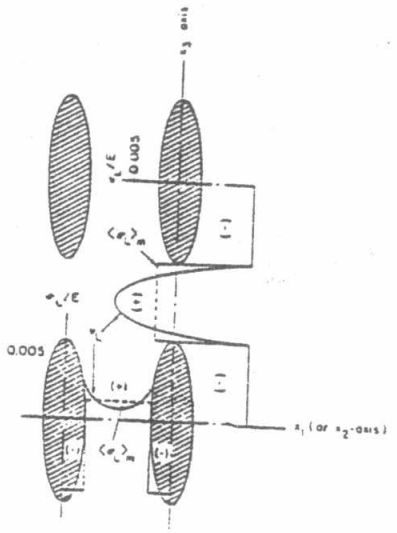

Figure 13 Schematic of the Predicted Residual Stresses (Arsenault and Taya, 1987) (Annealed 6061 Al, 17 vol.% SiC, aspect ratio =1.8 , Cooling from 430 °F).

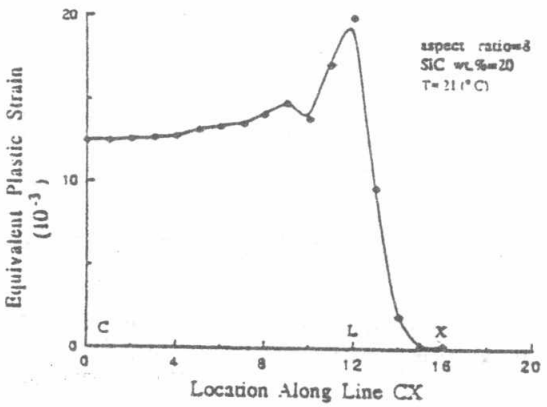

Figure 14 Equivalent Plastic Strain Distribution Along Line CX (in the Matrix) After Cooling.

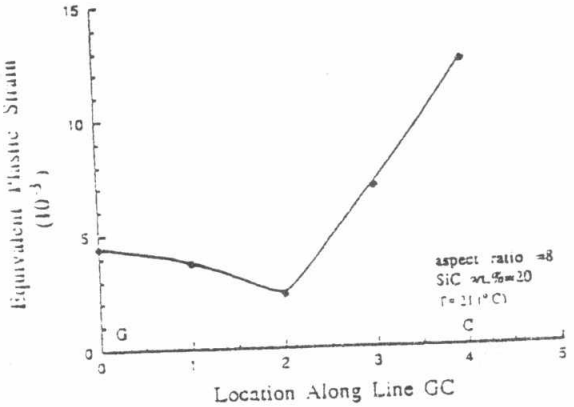

Figure 15 Equivalent Plastic Strain Distribution Along Line GC After Cooling.

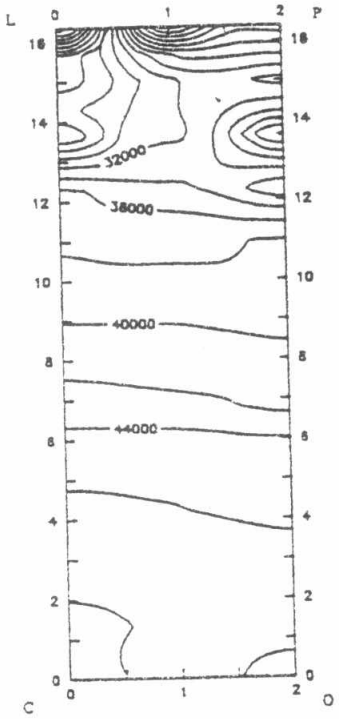

Figure 17 . Mises Stress Contours in Plane COPL (in the Whisker) After Cooling , (aspect ratio=8, SiC wt.%=20). (psi)

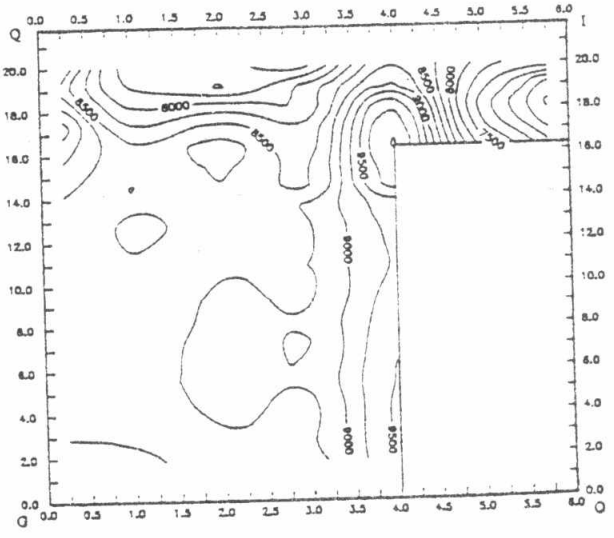

Figure 16 . Mises Stress Contours in Plane GOIQ (in the Matrix) After Cooling. (aspect ratio =8, SiC wt.% =20). (psi)

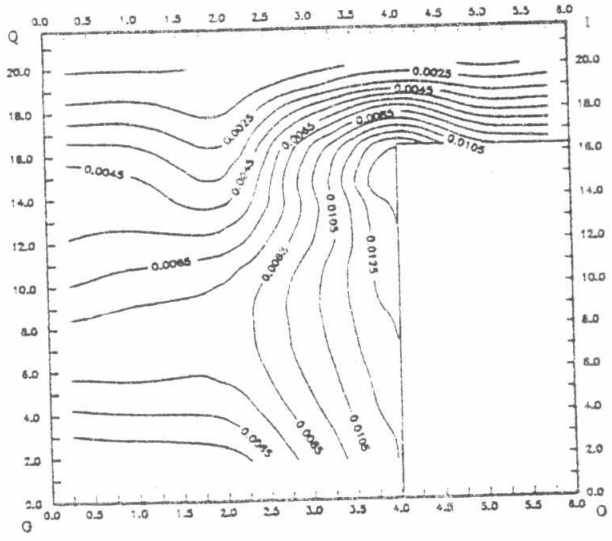

Figure 18 (a) Equivalent Plastic Strain Contours in Plane GOIQ (in the Matrix)After Cooling. (aspect ratio =8, SiC wt.% =20).

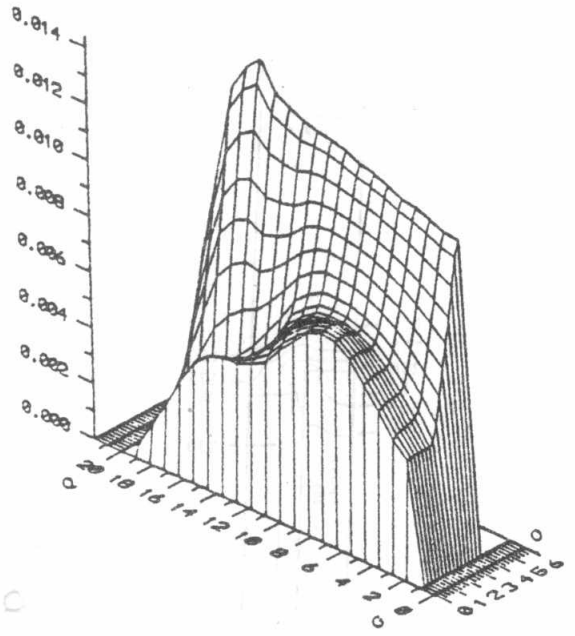

Figure 18 (b) Equivalent Plastic Strain Distribution in Plane GOIQ (in the Matrix) After Cooling. (aspect ratio =8, SiC wt.% =20).

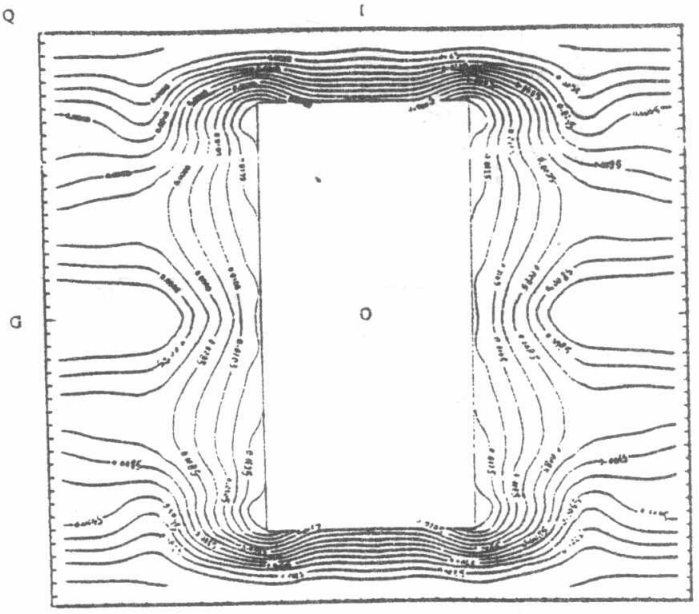

Figure 19 . Equivalent Plastic Strain Contours in Plane GOIQ (in the Matrix)After Cooling (aspect ratio =8, SiC wt.% =20)

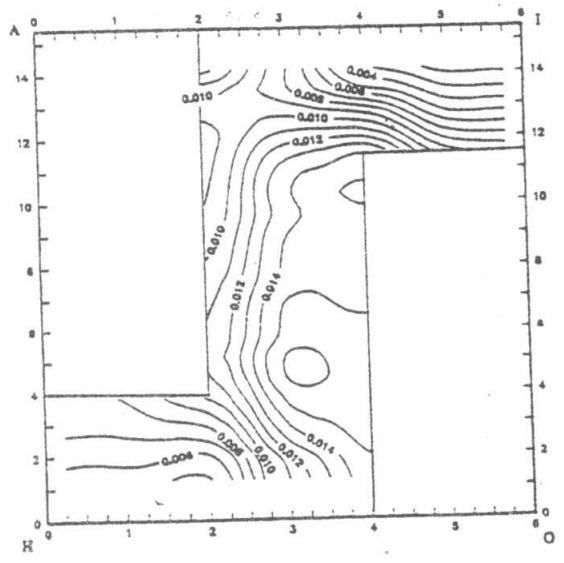

Figure 20 . Equivalent Plastic Strain Contours in Plane HOIA (in the Matrix) After Cooling. (aspect ratio =8, SiC wt.% =20).

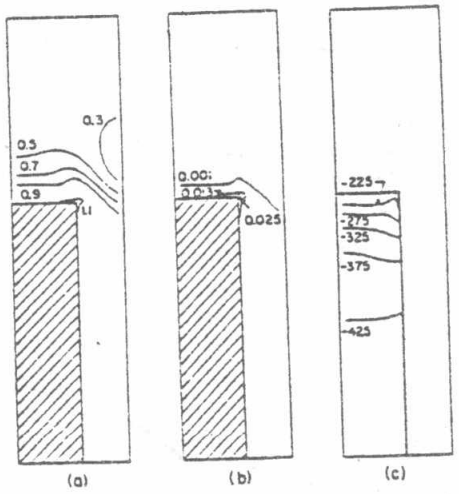

Figure 21 Contours of : a- Normalized Effective Residual Stress. b- Effective Plastic Strain. c- Residual Axial Stress (in MPa) in the Whisker. (Povirk et al., 1990) (20 vol.% SiC, aspect ratio =4, cooling from 700 °F).

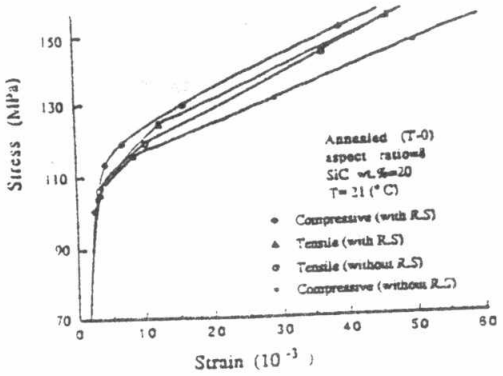

Figure 22 Predicted Stress-Strain Behavior of the Annealed Composite (with and without including Residual Stresses).

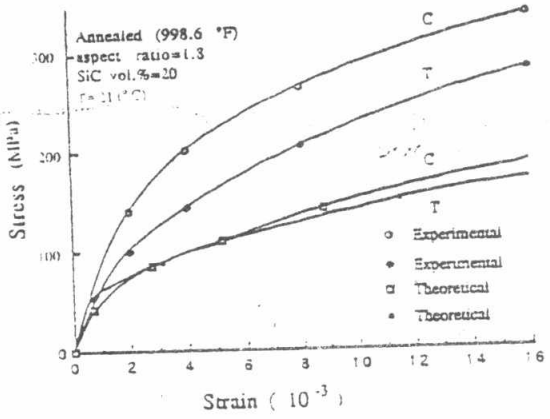

Figure 23 Predicted and Experimental (Arsenault and Taya,1987) Tensile and Compressive Behavior of the Annealed Composite.

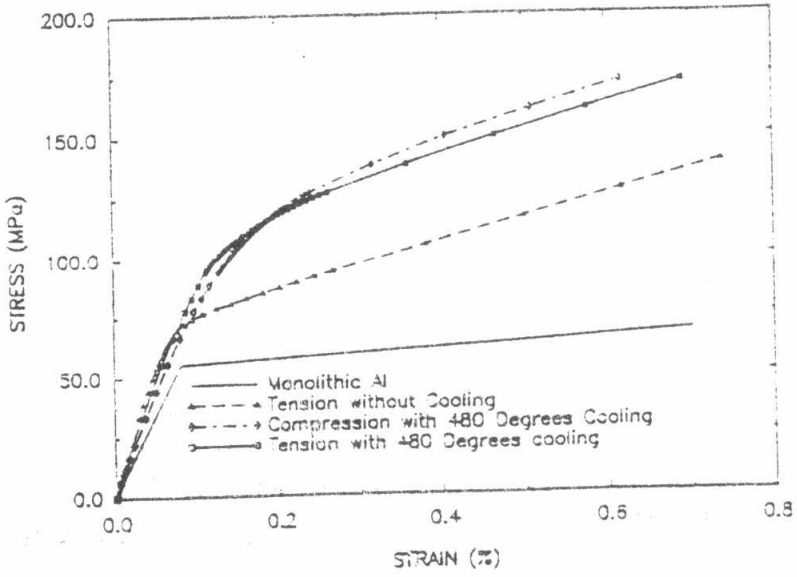

Fig. 24. Stress-Strain curves of annealed 6061 Al. with bilinear approximation and 20 vol.% SiCw /Al composite with ΔT=0 and 480 C (Shi et al. 1992)

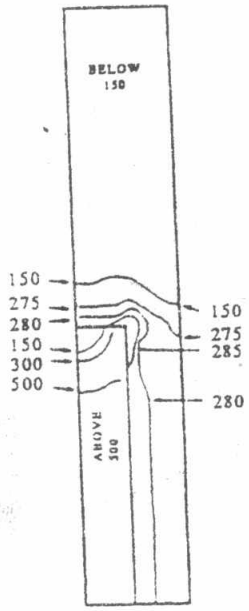

$\varepsilon_c = 0$

Fig. 25. Contours of constant Von-Mises effective stress in one quadrant of the composite unit cell due to thermal residual stress in 10 vol.% SiCw /6061 Al composite aspect ratio =6 (Dutta et al. 1993)